Supplemental material

Chen et al., https://doi.org/10.1083/jcb.201711065

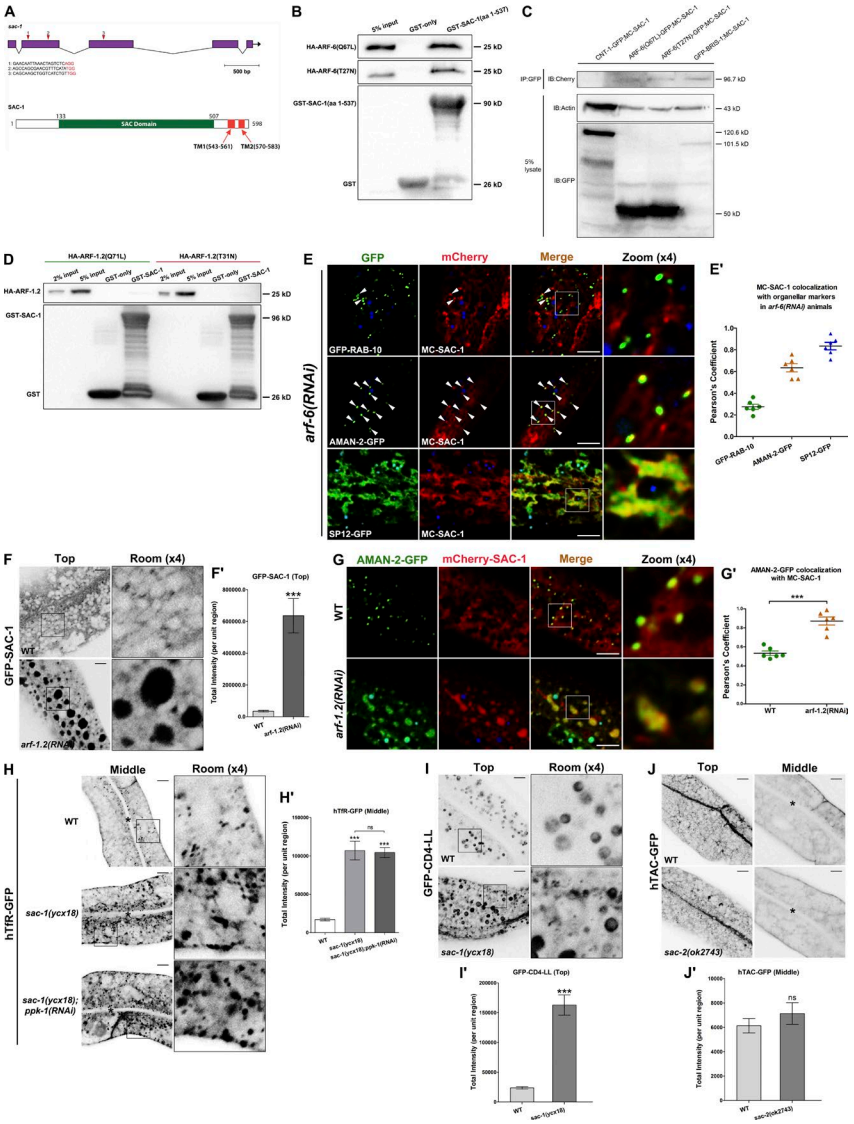

Figure S1. **The endosomal localization of mCherry-SAC-1 is impaired in *arf-6(RNAi)* animals, whereas the Golgi and ER labeling of mCherry-SAC-1 is intact in *arf-6(RNAi)* animals. (A)** *sac-1* open reading frame. Arrowheads above *sac-1* indicate three sgRNAs target locations in *sac-1(ycx18)* CRISPR/Cas9 intestine somatic mutants. SAC-1 is predicted to contain an N-terminal SAC domain and two C-terminal transmembrane domains (TM1 and TM2); amino acid numbers are indicated. **(B)** Glutathione beads loaded with GST and GST-SAC-1(aa 1–537) were incubated with in vitro–expressed HA-tagged ARF-6(Q67L) and ARF-6(T27N). Eluted proteins were separated on the SDS-PAGE gel and analyzed by Western blotting using anti–HA antibody. Input lanes contain in vitro expressed HA-tagged proteins in the binding assays (5%). **(C)** Coimmunoprecipitation experiments showing the interaction between ARF-6(Q67L) and SAC-1, ARF-6(T27N) and SAC-1, and BRIS-1 and SAC-1. **(D)** Glutathione beads loaded with GST and GST-SAC-1 were incubated with in vitro–expressed HA-tagged ARF-1.2(Q71L) and ARF-1.2(T31N). Eluted proteins were separated on the SDS-PAGE gel and analyzed by Western blotting using anti–HA antibody. Input lanes contain in vitro–expressed HA-tagged proteins in the binding assays (2% and 5%). **(E and E')** In *arf-6(RNAi)* animals, SAC-1 displayed little overlap with RAB-10–labeled endosomes, and SAC-1 overlaps significantly with the TGN marker AMAN-2 and the ER marker SP12. Arrowheads indicate positive overlap. Pearson's correlation coefficients for GFP and mCherry signals were calculated (n = 6 animals). **(F and F')** Loss of SAC-1 led to an accumulation of GFP-SAC-1. Error bars represent SEM (n = 18). Asterisks indicate the significant difference in the one-tailed Student's t test (***, P < 0.001). **(G and G')** In the absence of SAC-1, the overlap between AMAN-2-GFP and mCherry-SAC-1 was not affected. AMAN-2-GFP and mCherry-SAC-1 colocalize well in the enlarged structures. Pearson's correlation coefficients for GFP and mCherry signals were calculated (n = 6 animals). Error bars represent SEM. ***, P < 0.001. **(H and H')** hTfR-GFP accumulated in the cytosolic structures in *sac-1* mutants, and the overaccumulation phenotype of hTfR-GFP was not alleviated in *sac-1(−);ppk-1(RNAi)* animals. Error bars represent SEM (n = 18). Asterisks indicate significant differences in the one-tailed Student's t test (***, P < 0.001). **(I and I')** Loss of SAC-1 led to an accumulation of the nonrecycling cargo GFP-CD4-LL. Error bars represent SEM (n = 18). Asterisks indicate significant difference in the one-tailed Student's t test (***, P < 0.001). **(J and J')** Loss of SAC-2 had no significant effects on the distribution of hTAC-GFP. Asterisks in the panels indicate the intestinal lumen. Error bars represent SEM (n = 18). Bars, 10 µm.

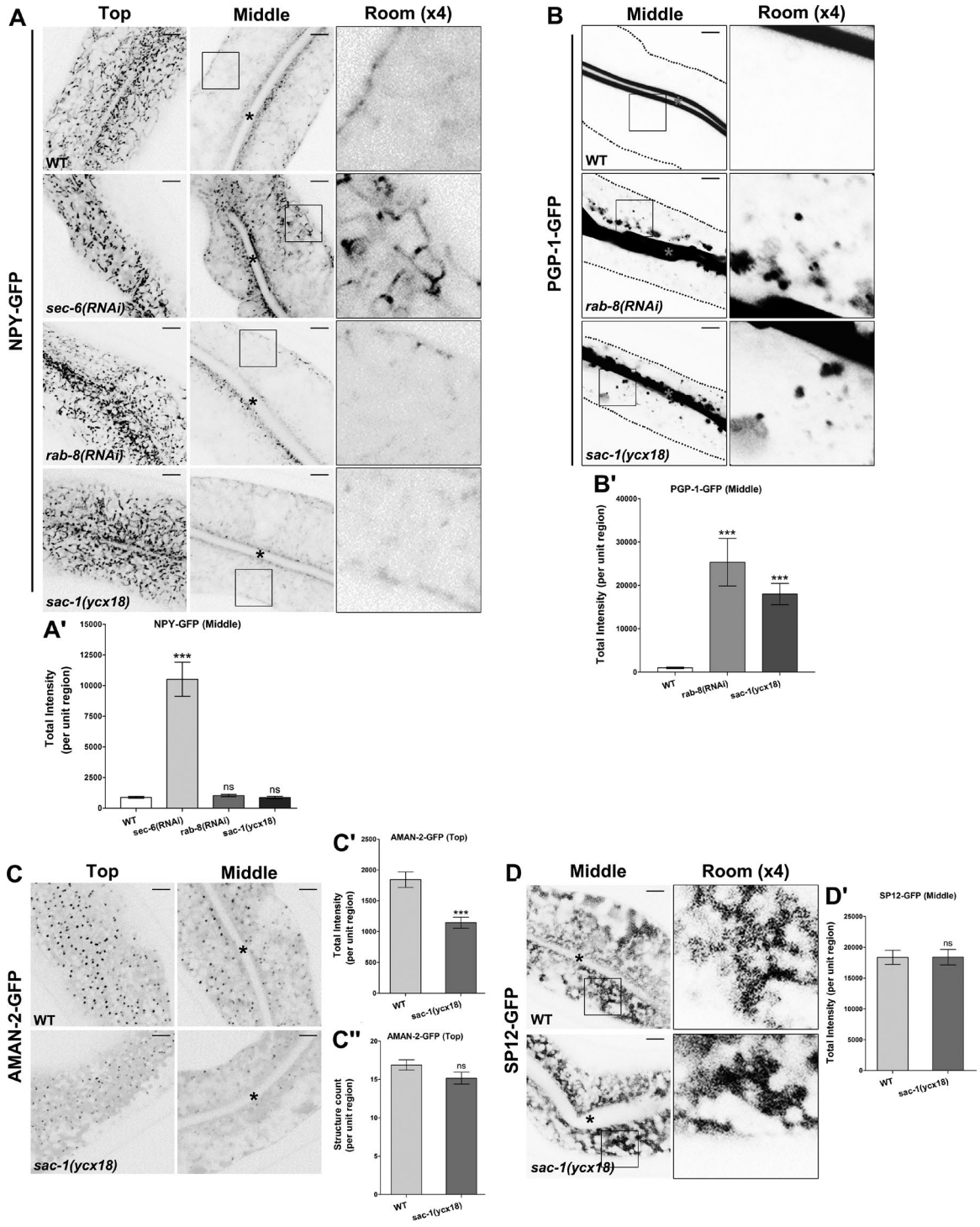

Figure S2. **The transport of basolateral secretory cargo NPY-GFP is not affected in *sac-1(ycx18)* animals, whereas apical secretory cargo protein PGP-1-GFP accumulates in *sac-1(ycx18)* mutants. (A and A')** In the top focal plane, NPY-GFP–labeled tubular structures were severely affected in *sec-6(RNAi)* animals. In the middle focal plane, NPY-GFP overaccumulated in the cytosolic structures. An approximately 10-fold increase of total NPY-GFP intensity was observed. In contrast, in *rab-8(RNAi)* or *sac-1(ycx18)* cells, the NPY-GFP labeling pattern remains intact. Asterisks in the panels indicate the intestinal lumen. Error bars represent SEM (n = 18). Asterisks indicate the significant difference in the one-tailed Student's t test (***, $P < 0.001$). **(B and B')** In *sac-1(ycx18)* mutants and *rab-8(RNAi)* animals, apical secretory cargo PGP-1-GFP strongly accumulated in the intracellular aggregates. Red asterisks in the panels indicate the intestinal lumen. Error bars represent SEM (n = 18). Asterisks indicate significant differences in the one-tailed Student's t test (***, $P < 0.001$). **(C–C")** AMAN-2-GFP–labeled puncta intensity was decreased in *sac-1* mutants. However, the subcellular distribution of AMAN-2-GFP–labeled puncta was not obviously disturbed in *sac-1* mutant animals. Asterisks in the panels indicate the intestinal lumen. Error bars represent SEM (n = 18). Asterisks indicate significant differences in the one-tailed Student's t test (***, $P < 0.001$). **(D and D')** SP12-GFP–labeled ER structures were not affected in *sac-1* mutants. Asterisks in the panels indicate intestinal lumen. Error bars represent SEM (n = 18). Bars, 10 µm.

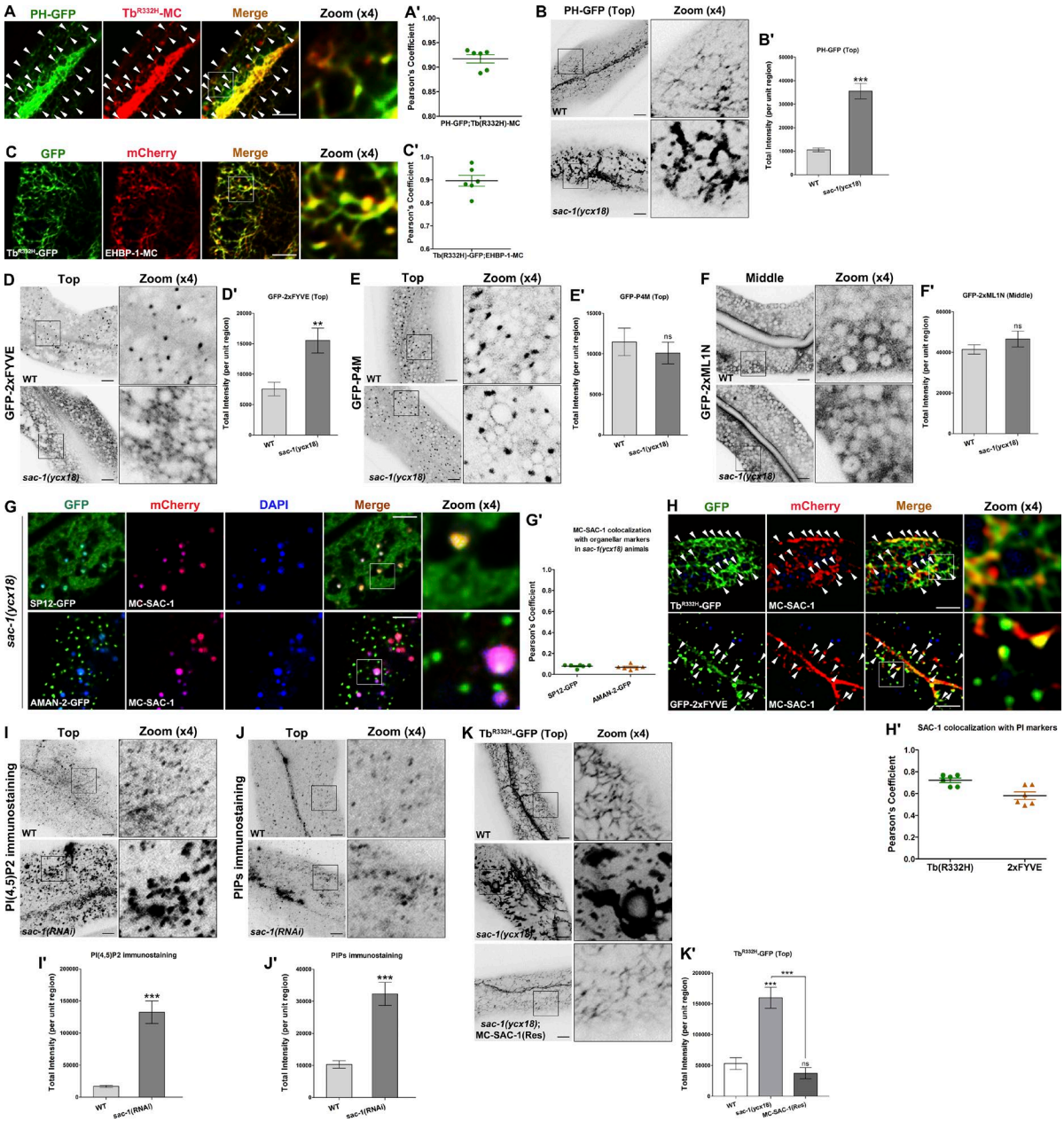

Figure S3. **The level of PI(4,5)P2 in the basolateral endosomes is promoted in *sac-1(RNAi)* animals, and the level of total PIPs increases moderately in *sac-1(RNAi)* animals. (A and A')** Tb^{R332H}-mCherry colocalizes extensively with PI(4,5)P2 biosensor PH-GFP (Pearson's correlation coefficient, ∼92.7%). Arrowheads indicate positive overlap. Pearson's correlation coefficients for GFP and mCherry signals were calculated (n = 6 animals). **(B and B')** In the absence of SAC-1, PH-GFP overaccumulated in the intracellular aggregates. Error bars represent SEM (n = 18). Asterisks indicate significant differences in the one-tailed Student's t test (***, P < 0.001). **(C and C')** Tb^{R332H}-GFP and EHBP-1-mCherry colocalize well in the tubular and punctate structures. Pearson's correlation coefficients for GFP and mCherry signals were calculated (n = 6 animals). **(D and D')** The mean intensity of GFP-2xFYVE–labeled puncta increased significantly in *sac-1* mutants. Error bars represent SEM (n = 18). Asterisks indicate significant differences in the one-tailed Student's t test (**, P < 0.01). **(E and E')** PI(4)P marker GFP-P4M had no significant change in the distribution or labeling intensity in *sac-1* mutants. Error bars represent SEM (n = 18). **(F and F')** The subcellular distribution of PI(3,5)P2 marker GFP-2xML1N was not affected by the loss of SAC-1. Error bars represent SEM (n = 18). **(G and G')** In *sac-1(ycx18)* animals, AMAN-2-GFP and SP12-GFP displayed little overlap with mCherry-RAB-10. Pearson's correlation coefficients for GFP and mCherry signals were calculated (n = 6 animals). **(H and H')** mCherry-SAC-1 colocalized well with Tb^{R332H}-GFP on endosomes (Pearson's coefficient, ∼72%). Also, mCherry-SAC-1 partially overlapped with GFP-2xFYVE (Pearson's coefficient, ∼58%). Arrowheads indicate positive overlap. Pearson's correlation coefficients for GFP and mCherry signals were calculated (n = 6 animals). **(I and I')** Compared with wild-type animals, the intensity of PI(4,5)P2 antibody staining in the basolateral endosomes was promoted in *sac-1(RNAi)* animals. Error bars represent SEM (n = 18). Asterisks indicate the significant differences in the one-tailed Student's t test (***, P < 0.001). **(J and J')** In *sac-1(RNAi)* animals, the intensity of PIPs antibody staining increased moderately. Error bars represent SEM (n = 18). Asterisks indicate significant differences in the one-tailed Student's t test (***, P < 0.001). **(K and K')** Transgenic expression of a CRISPR/Cas9 editing–resistant mCherry-SAC-1 rescued the accumulation phenotype of Tb^{R332H}-GFP in *sac-1(ycx18)* mutants, where the Tb^{R332H}-GFP intensity was even lower than that of wild-type animals. Error bars represent SEM (n = 18). Asterisks indicate significant differences in the one-tailed Student's t test (***, P < 0.001). Bars, 10 µm.

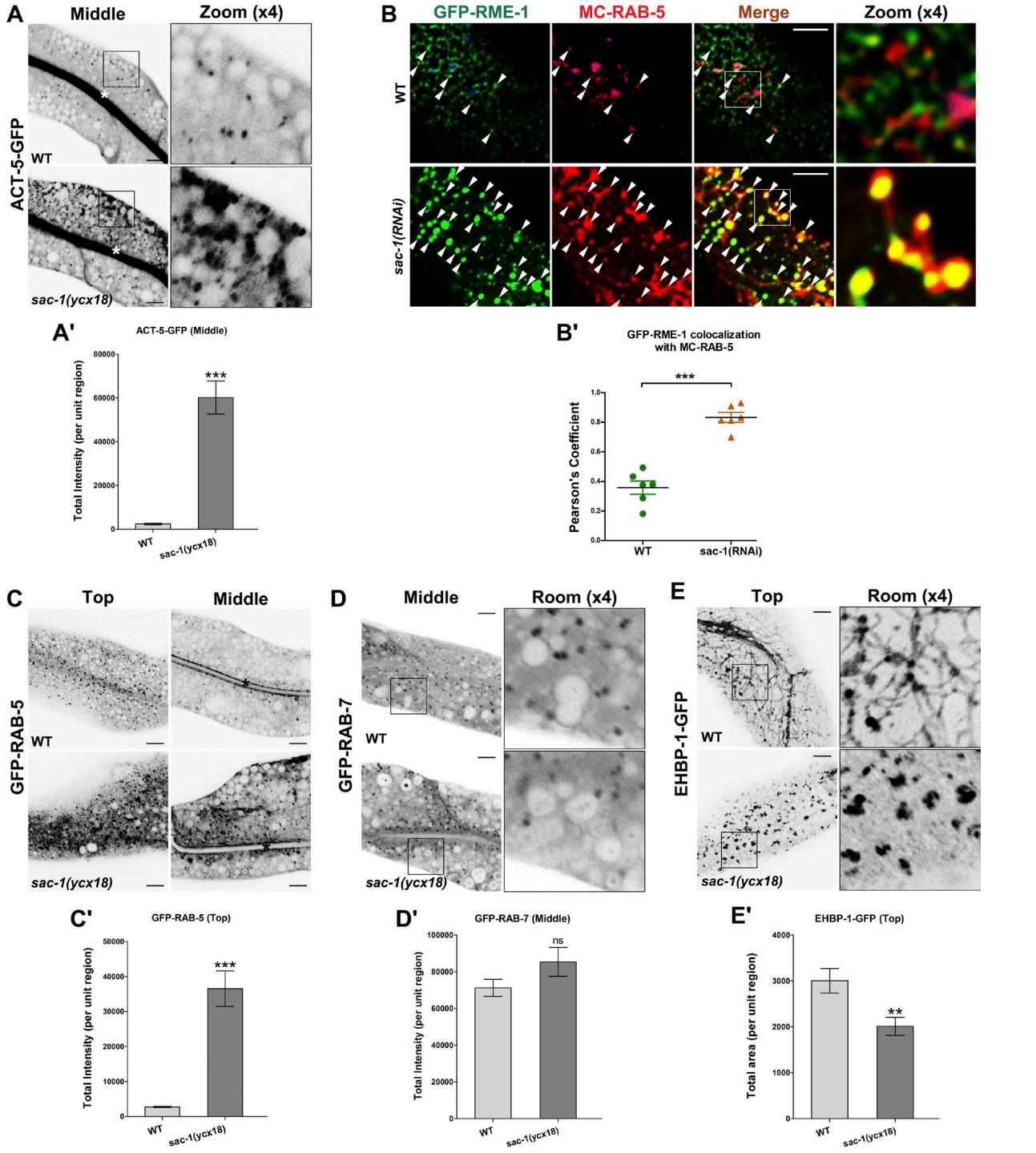

Figure S4. **The recycling marker GFP-RME-1 accumulates in RAB-5–positive endosomes in SAC-1–depleted cells. (A and A')** ACT-5-GFP–labeled puncta overaccumulated extensively in *sac-1* mutants. Asterisks in the panels indicate intestinal lumen. Error bars represent SEM (n = 18). Asterisks indicate significant differences in the one-tailed Student's t test (***, P < 0.001). **(B and B')** In *sac-1(RNAi)* animals, the overlap between GFP-RME-1 and mCherry-RAB-5 was promoted. Arrowheads indicate positive overlap. Pearson's correlation coefficients for GFP and mCherry signals were calculated (n = 6 animals). Error bars represent SEM. ***, P < 0.001. **(C and C')** GFP-RAB-5–labeled early endosomes accumulated upon loss of SAC-1. Asterisks in the panels indicate intestinal lumen. Error bars represent SEM (n = 18). Asterisks indicate significant differences in the one-tailed Student's t test (***, P < 0.001). **(D and D')** RAB-7–labeled structures distribution was not perturbed by the loss of SAC-1. Error bars represent SEM (n = 18). **(E and E')** The RAB-10 effector EHBP-1–labeled recycling tubular network was disrupted in *sac-1* mutants. Error bars represent SEM (n = 18). Asterisks indicate a significant difference in the one-tailed Student's t test (**, P < 0.01). Bars, 10 µm.

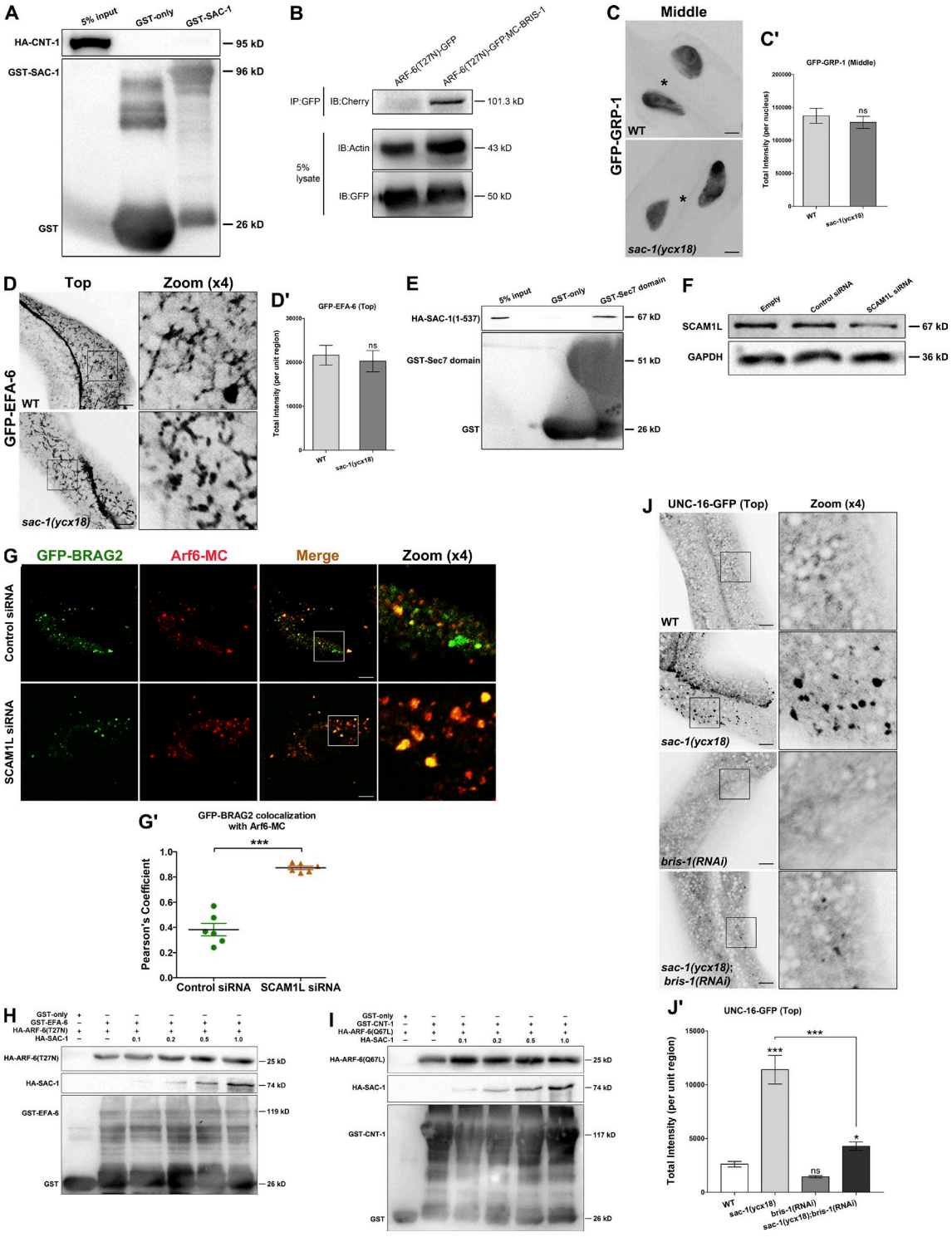

Figure S5. **Loss of SCAM1L boosts the colocalization between GFP-BRAG2 and Arf6-mCherry, and SAC-1 fails to outcompete ARF-6(T27N) for interaction with EFA-6. (A)** No interaction between GST-SAC-1 and HA-CNT-1 was observed. **(B)** Coimmunoprecipitation experiments showing the interaction between ARF-6(T27N) and BRIS-1. **(C and C')** The distribution of GFP-GRP-1 within nuclei was not affected in *sac-1* mutants. Error bars represent SEM (n = 18). **(D and D')** The subcellular distribution of GFP-EFA-6 was not significantly disturbed by the loss of SAC-1. Error bars represent SEM (n = 18). **(E)** The Sec7 domain mediates the interaction of BRIS-1 with SAC domain (aa 1–537). **(F)** The knockdown efficiency of the SCAM1L siRNA was analyzed by Western blotting using anti–SCAM1L antibody. **(G and G')** In the absence of SCAM1L, the overlap between GFP-BRAG2 and Arf6-mCherry was greatly increased. Pearson's correlation coefficients for GFP and mCherry signals were calculated (n = 18 cells). Error bars represent SEM: ***P < 0.001. **(H)** SAC-1 failed to outcompete ARF-6(T27N) for interaction with EFA-6, as determined by GST pull-down. **(I)** SAC-1 failed to outcompete ARF-6(Q67L) for interaction with CNT-1, as determined by GST pull-down. **(J and J')** Loss of SAC-1 resulted in the overaccumulation of UNC-16-positive structures. However, the accumulation phenotype of UNC-16-GFP was significantly eased by the simultaneous knockdown of BRIS-1. Error bars represent SEM (n = 18). Asterisks indicate significant differences in the one-tailed Student's t test (*, P < 0.05; ***P < 0.001). Bars, 10 µm.

Table S1. **Transgenic and mutant strains**

Strains	Reference
ycx18[pvha6::Cas9::tbb-2 3'+pU6-sac-1::sgRNA I&II&III]	This study
ycxIs222[pvha6::Tubby-PH(R332H)::GFP]	Liu et al., 2018
ycxIs12[pvha6::EHBP-1::GFP]	Wang et al., 2016
ycxIs100[pvha6::GFP::Utrophin(CH)]	This study
ycxIs51[pvha6::EMTB::3xGFP]	Wang et al., 2016
ycxEx839[pvha6::GFP::BRIS-1]	This study
ycxEx858[pvha6::GFP::EFA-6]	This study
ycxEx859[pvha6::GFP::GRP-1]	This study
ycxEx838[pvha6::GFP::2xML1N]	This study
ycxEx853[pvha6::GFP::P4M]	This study
ycxEx263[pvha6::GFP::2xFYVE]	Liu et al., 2018
ycxEx288[pvha6::mCherry::2xFYVE]	Wang et al., 2016
ycxEx999[pvha6::GFP::SAC-1]	This study
ycxEx1000[pvha6::mCherry::SAC-1]	This study
ycxEx1051[pvha6::SAC-1]	This study
ycxEx809[pvha6::mCherry::BRIS-1]	This study
pwIs717[pvha6::hTfR::GFP]	Chen et al., 2006
pwIs112[pvha6::hTAC::GFP]	Chen et al., 2006
pwIs503[pvha6::AMAN-2::GFP]	Shi et al., 2009
pwIs601[pvha6::ARF-6::GFP]	Shi et al., 2012
pwIs1196[pvha-6::ssGFP::CD4-dileucine]	Gleason et al., 2016
pwIs72[pvha6::GFP::RAB-5]	Chen et al., 2006
pwIs846[pvha-6::mCherry::RAB-5]	Wang et al., 2016
pwIs170[pvha6::GFP::RAB-7]	Chen et al., 2006
pwIs206[pvha6::GFP::RAB-10]	Chen et al., 2006
ycxEx684[pvha-6::mCherry::RAB-10]	This study
pwIs87[pvha6::GFP::RME-1]	Chen et al., 2006
pwIs314[pvha6::ACT-5::GFP]	This study
pwIs526[pvha6::SP12::GFP]	This study
pwIs445[pvha6::PH::GFP]	Shi et al., 2012
dkIs37[pvha6::GFP::PGP-1]	Sato et al., 2007
ycxIs833[pvha6::EHBP-1::mCherry]	Shi et al., 2010
ycxEx1032[pvha6::GFP::HMP-1]	Liu et al., 2018
ycxEx1000[pvha6::ARF-6(Q67L)::mCherry]	This study
ycxEx1039[pvha6::NPY::GFP]	This study
arf-6(tm1447)	Shohei Mitani, Tokyo Women's Medical University School of Medicine, Tokyo, Japan, Japanese National Bioresource Project for the Experimental Animal "Nematode *C. elegans*"

Provided online is Table S2 as a PDF, showing the alignment of *C. elegans* SAC-1 and the closely related homologues in human and yeast.

References

Chen, C.C., P.J. Schweinsberg, S. Vashist, D.P. Mareiniss, E.J. Lambie, and B.D. Grant. 2006. RAB-10 is required for endocytic recycling in the Caenorhabditis elegans intestine. *Mol. Biol. Cell.* 17:1286–1297. https://doi.org/10.1091/mbc.E05-08-0787

Gleason, A.M., K.C. Nguyen, D.H. Hall, and B.D. Grant. 2016. Syndapin/SDPN-1 is required for endocytic recycling and endosomal actin association in the C. elegans intestine. *Mol. Biol. Cell.* mbc.E16-02-0116.

Liu, H., S. Wang, W. Hang, J. Gao, W. Zhang, Z. Cheng, C. Yang, J. He, J. Zhou, J. Chen, and A. Shi. 2018. LET-413/Erbin acts as a RAB-5 effector to promote RAB-10 activation during endocytic recycling. *J. Cell Biol.* 217:299–314. https://doi.org/10.1083/jcb.201705136

Sato, T., S. Mushiake, Y. Kato, K. Sato, M. Sato, N. Takeda, K. Ozono, K. Miki, Y. Kubo, A. Tsuji, et al. 2007. The Rab8 GTPase regulates apical protein localization in intestinal cells. *Nature.* 448:366–369. https://doi.org/10.1038/nature05929

Shi, A., L. Sun, R. Banerjee, M. Tobin, Y. Zhang, and B.D. Grant. 2009. Regulation of endosomal clathrin and retromer-mediated endosome to Golgi retrograde transport by the J-domain protein RME-8. *EMBO J.* 28:3290–3302. https://doi.org/10.1038/emboj.2009.272

Shi, A., C.C. Chen, R. Banerjee, D. Glodowski, A. Audhya, C. Rongo, and B.D. Grant. 2010. EHBP-1 functions with RAB-10 during endocytic recycling in Caenorhabditis elegans. *Mol. Biol. Cell.* 21:2930–2943. https://doi.org/10.1091/mbc.E10-02-0149

Shi, A., O. Liu, S. Koenig, R. Banerjee, C.C. Chen, S. Eimer, and B.D. Grant. 2012. RAB-10-GTPase-mediated regulation of endosomal phosphatidylinositol-4,5-bisphosphate. *Proc. Natl. Acad. Sci. USA.* 109:E2306–E2315. https://doi.org/10.1073/pnas.1205278109

Wang, P., H. Liu, Y. Wang, O. Liu, J. Zhang, A. Gleason, Z. Yang, H. Wang, A. Shi, and B.D. Grant. 2016. RAB-10 Promotes EHBP-1 Bridging of Filamentous Actin and Tubular Recycling Endosomes. *PLoS Genet.* 12:e1006093. https://doi.org/10.1371/journal.pgen.1006093